Global sensitivity analysis of a model for silicon nanoparticle synthesis

William J. Menz, George P. E. Brownbridge, Markus Kraft

released: January 29, 2014

[1] Department of Chemical Engineering
and Biotechnology
University of Cambridge
New Museums Site
Pembroke Street
Cambridge, CB2 3RA
United Kingdom
E-mail: mk306@cam.ac.uk

Preprint No. 141

UNIVERSITY OF
CAMBRIDGE

Abstract

This paper presents a global sensitivity analysis of the detailed population balance model for silicon nanoparticle synthesis of Menz & Kraft (2013, *Combustion & Flame*, **160**:947–958). The model consists of a gas-phase kinetic model, fully coupled with a particle population balance. The sensitivity of the model to its seven adjusted parameters was analysed in this work using a High Dimensional Model Representation (HDMR). An algorithm is implemented to generate response surface polynomials with automatically selected order based-on their coefficient of determination. A response surface is generated for 19 different experimental cases across a range of process conditions and reactor configurations. This enables the sensitivity of individual experiments to certain parameters to be assessed. The HDMR reveals that particle size was most sensitive to the heterogeneous growth process, while the particle size distribution width is also strongly dependent on the rate of nucleation.

Contents

1 Introduction

Knowledge of the properties of silicon has underpinned the revolution of information technology. A great deal of study has therefore been undertaken into its synthesis, purification and resultant properties. Silicon nanoparticles were first made in the late 1970's [28] and since then, have been the subject of considerable work towards improving their manufacture and identifying potential applications.

Gas-phase, laser and plasma synthesis of particles are the most common methods with which silicon nanoparticles are manufactured [21]. In general, these processes begin with silane (SiH_4), which may be decomposed by thermal, laser or microwave radiation [4, 14, 29]. The decomposition of silane forms reactive silicon hydrides, which combine with each other to nucleate into silicon nanoparticles [38].

Various models–from gas-phase kinetic to particle population balances–have been proposed to describe the formation of nanoparticles from silane [24, 30, 38]. In all of these models, it is common to find model parameters which have uncertain values. Examples include empirical expressions for sintering [6, 24, 36].

In some cases, it is possible to estimate these values by trial-and-error [15]. However, for a non-linear model with many unknown parameters, this process becomes difficult. Systematic parameter estimation can be used to move from by-hand guesswork to computer-based solutions. For example, a model implemented in Excel® could use the GOALSEEK or SOLVER functionality to arrive at better input parameter values.

There are a range of optimisation techniques which can be used to improve model values [17]. Low-discrepancy sampling can be used to evaluate the model response over a space of parameter values [3]. Gradient-search methods such as the simultaneous perturbation stochastic approximation (SPSA) algorithm can locate local and global minima [6, 24]. Response surfaces, or surrogate models, can also be generated from low-discrepancy sampling, yielding a computationally-efficient approximations of the true model [13]. Then, Markov Chain Monte Carlo (MCMC) sampling and Bayesian analyses are often applied to assess the credible regions in which the optimal parameter values may lie [13, 27].

Recently, a detailed model for silicon nanoparticle synthesis was presented [22]. The model incorporates a gas-phase kinetic model, fully-coupled with a particle population balance. In its original development, systematic parameter estimation was used to optimise the model's seven parameters with respect to experimental data across a range of different process conditions. However, the relative importance of each parameter in the objective function was not quantitatively addressed in this work. Nor was the influence of particular experiments on the objective function. These open questions should be addressed in order to further assess the physical relevance of the model as well as its sensitivity to input parameters.

Due to the variety of solution methods for population balance models, there are a range of different approaches for studying the sensitivity of the model's parameters. Vikhansky and Kraft [40, 41] demonstrated use of a gradient search method to assess the sensitivity of stochastic (Monte Carlo) solution methodologies as applied to population balances equations. In complex models, a simple scan of the parameter space can also be used [18, 36]. An excellent review of sensitivity analysis methods is given by Tomlin [39].
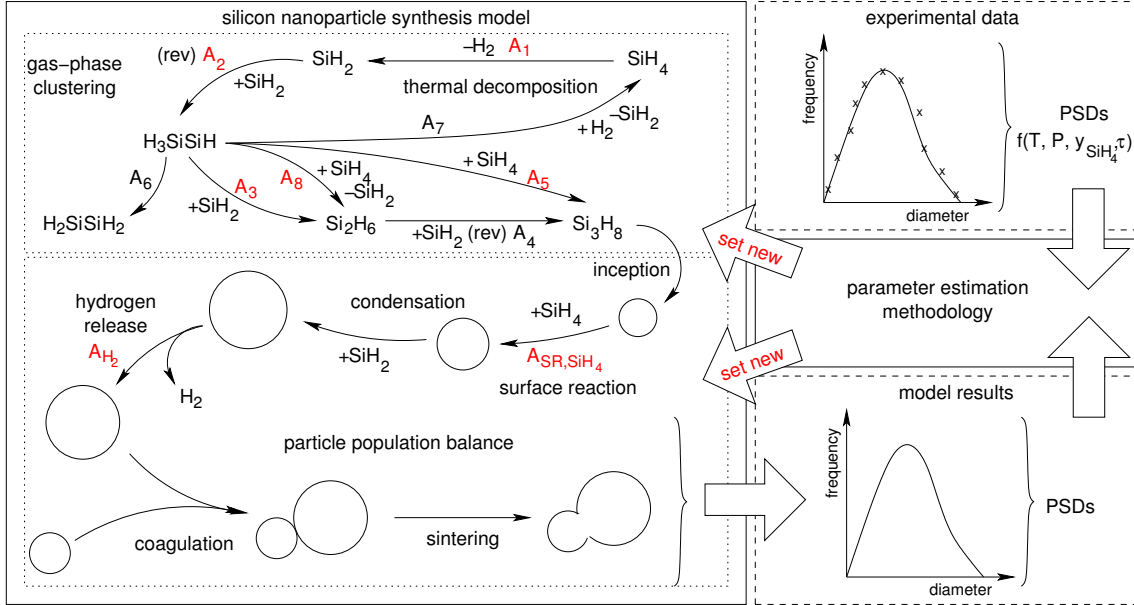
3

Figure 1: *Schematic of the information transfer between the models, the parameter estimation methodology and experimental sources. The quantities highlighted in red refer to the adjusted parameters.*

The purpose of this work is to investigate the estimated parameters in model of Menz and Kraft [22] for silicon nanoparticle synthesis. A global sensitivity analysis will be conducted using HDMR response surfaces in order to elucidate the influence of each parameter in the optimisation. This will illustrate an alternative approach through which sensitivity analyses can be conducted, not as yet used in this community. Finally, the sensitivity analysis will also be applied to gain additional physical insight into the model.

The structure of this paper is as follows. A brief description of the model is given in Section 2, including the gas-phase (Section 2.1) and the population balance (Section 2.2). The techniques used for parameter estimation and sensitivity analysis are presented in Section 3. The results from the sensitivity analysis are given and discussed in Section 4.

2 Model

The model for silicon nanoparticle synthesis is composed of a gas-phase kinetic model and a particle population balance model. A full formulation of the model is given in [22], however a brief description is given here. In the original development of the model, parameter estimation was used to optimise gas-phase and particle-phase parameters with respect to experimental results from the literature. This process is illustrated in Figure 1.

2.1 Gas-phase model

The bulk decomposition of silane can be described as the bimolecular expression [32]:

$$\text{SiH}_4 + \text{M} \rightarrow \text{SiH}_2 + \text{H}_2 + \text{M} \tag{1}$$

where M is a third body. It is well-understood that silane decomposition proceeds through a series of intermediate gas-phase species, such as silylene (SiH_2) and higher silenes/silanes. For this model, the mechanism of Ho et al. [11] is adopted. The mechanism has eight core reactions, mostly described by Lindemann falloff expressions. Pre-exponential factors for five of the reactions were adjusted from their initial values. The equations describing the rate of change of chemical species due to these reactions are solved using a conventional ordinary differential equation (ODE) solver.

2.2 Particle population balance model

The binary-tree particle model of Sander et al. [34] is used in this work. Each particle P_q is represented as:

$$P_q = P_q\left(p_1, \ldots, p_{n_q}, \mathbf{C}\right) \tag{2}$$

where particle P_q contains n_q primary particles p_x. $\mathbf{C}$ is a lower-diagonal matrix representing the common surface area between two primary particles. Each primary particle is described by the number of silicon atoms η_{Si} and hydrogen atoms η_{H}:

$$p_x = p_x\left(\eta_{\text{Si}}, \eta_{\text{H}}\right) \tag{3}$$

All other properties of the particle are derived from this representation. A full mathematical formulation of the model is given in [22] and [35]. Particle processes can change the type-space of a particle in a variety of different ways. The processes included in the model for silicon nanoparticle synthesis are listed in Table 1 and described below.

Inception
> A collision of a silylene (e.g. SiH_2) species with another silylene or silene species will form a particle. The rate of inception dependent on the critical nucleus diameter, a quantity which may be estimated using macroscopic properties of silicon and the process conditions [22]. When the diameter of the particle to be incepted is greater than the critical diameter, the rate of inception is calculated using the transition regime coagulation kernel [25].

Surface reaction
> In this context, surface reactions refer to the heterogeneous reaction of silanes (SiH_4, Si_2H_6, Si_3H_8) on the particle surface. Silanes must proceed through an energy barrier in order for the reaction to proceed [12]. Hence, the rate of surface reaction is represented by a Arrhenius rate constant [11]. It is also proportional to the particle surface area [22]. In the population balance model, a surface reaction event also causes rounding of joined primaries. This is represented by the transformation $\mathbf{C} \rightarrow \mathbf{C}'$.

5

Table 1: *Particle processes included in the population balance model.*

Process	Reaction
Inception	$\mathrm{Si}_i\mathrm{H}_j\mathrm{B} + \mathrm{Si}_k\mathrm{H}_l \to P(\eta_{\mathrm{Si}} = i+k, \eta_{\mathrm{H}} = j+l, \mathbf{C})$
Surface reaction	$P(\ldots, p_x(\eta_{\mathrm{Si}}, \eta_{\mathrm{H}}), \ldots, \mathbf{C}) + \mathrm{Si}_i\mathrm{H}_{2i+2}$ $\to P(\ldots, p_x(\eta_{\mathrm{Si}} + i, \eta_{\mathrm{H}} + 2), \ldots, \mathbf{C}') + i\mathrm{H}_2$
Condensation ($j \neq i+2$)	$P(\ldots, p_x(\eta_{\mathrm{Si}}, \eta_{\mathrm{H}}), \ldots, \mathbf{C}) + \mathrm{Si}_i\mathrm{H}_j$ $\to P(\ldots, p_x(\eta_{\mathrm{Si}} + i, \eta_{\mathrm{H}} + j), \ldots, \mathbf{C}')$
Hydrogen release	$P(\ldots, p_x(\eta_{\mathrm{Si}}, \eta_{\mathrm{H}}), \ldots, \mathbf{C})$ $\to P(\ldots, p_x(\eta_{\mathrm{Si}}, \eta_{\mathrm{H}} - 2), \ldots, \mathbf{C}) + \mathrm{H}_2$
Coagulation	$P_q(p_1, \ldots, p_{n_q}, \mathbf{C}_q) + P_r(p_1, \ldots, p_{n_r}, \mathbf{C}_r)$ $\to P_s(p_1, \ldots, p_{n_q}, p_{n_q+1}, \ldots, p_{n_q+n_s}, \mathbf{C}_s)$
Sintering ($n' \leq n$)	$P(p_1, \ldots, p_n, \mathbf{C}) \to P(p_1, \ldots, p_{n'}, \mathbf{C}')$

Condensation

Silenes (e.g. $\mathrm{H}_2\mathrm{SiSiH}_2$) and silylenes (e.g. SiH_2) react with particle surfaces through a condensation process. That is, their rate of reaction is given by a collision kernel, here the free-molecular kernel. It is assumed that they stick with probability 1.0 and that there is no energy barrier to reaction.

Hydrogen release

Particles must release hydrogen in order to maintain a stable crystal structure when growing. The rate of hydrogen desorption is proportional to the coverage of hydrogen on the particle surface as well as an Arrhenius rate constant [37]. In this model, the coverage is approximated by the ratio of number of hydrogen atoms to number of silicon atoms in each particle.

Coagulation

The rate of coagulation is dependent on the Knudsen number, and is given by the transition kernel. In a coagulation event, the particle trees are added to each other, preserving the particle size and connectivity information held in the state-space.

Sintering

Adjacent primary particles may sinter through a grain-boundary diffusion process. The common surface element of connected primaries p_x and p_y, C_{xy}, will decrease until it is sufficiently close to the equivalent spherical area of the two primaries. Then, the primaries are merged into a single primary particle. This occurs as a continuous process throughout the tree of primaries in the computational particle.

A stochastic numerical method is employed to solve the population balance model. This method has been well-documented [1, 26, 35] and takes advantage of various features

Table 2: *Overview of adjusted parameters.*

j	Symbol	Phase	Description
1	$A_{1,\text{LP}}$	Gas	Low-pressure pre-exponential factor for Reaction 1
2	$A_{2,\text{LP}}$	Gas	Low-pressure pre-exponential factor for Reaction 2
3	$A_{3,\text{LP}}$	Gas	Low-pressure pre-exponential factor for Reaction 3
4	$A_{5,\text{LP}}$	Gas	Low-pressure pre-exponential factor for Reaction 5
5	$A_{8,\text{rev}}$	Gas	Reverse pre-exponential factor for Reaction 8
6	$A_{\text{SR},\text{SiH}_4}$	Particle	Pre-exponential factor for SiH_4 surface reactions
7	A_{H_2}	Particle	Pre-exponential factor for H_2 release

such as linear process deferment [31], a binary tree cache [10] and the concept of majorant rates with fictitious jumps [7] to accelerate the solution of the population balance model. Coupling with the gas-phase is accomplished using the technique of operator splitting [5, 35].

3 Parameter estimation

In the original development of the model, parameter estimation was used to obtain suitable fit of the model response to experimental results. Seven parameters were identified for estimation. The physical and numerical meaning of these parameters are given in Figure 1 and Table 2 respectively. This results in a parameter vector given by:

$$\theta = (A_{1,\text{LP}}, A_{2,\text{LP}}, A_{3,\text{LP}}, A_{5,\text{LP}}, A_{8,\text{rev}}, A_{\text{SR},\text{SiH}_4}, A_{\text{H}_2}) \tag{4}$$

The optimal set of parameters (θ^*) is reliant on measuring the distance of the model response from the experimental results. To do this, a least-squares objective function, $\Phi(\theta)$, was formulated:

$$\Phi(\theta) = \sum_{i=1}^{N_{\text{exp}}} \left(\eta_i^{\text{exp}} - \eta_i^{\text{sim}}(\theta) \right)^2 \tag{5}$$

where η_i^{exp} is an experimental response, and η_i^{sim} is obtained from the model for the corresponding experiment. The number of experiments used in the optimisation is given by N_{exp}. A staged optimisation procedure was used to find the optimal set of parameters $\hat{\theta}$, with numerical results given in [22].

3.1 High Dimensional Model Representation

In this work, we are interested in the sensitivity of the model and its parameters near the optimal found in previous work. The global sensitivities can be calculated from a High Dimensional Model Representation (HDMR) [33]. A HDMR is a form of response surface, or surrogate model. Its main feature is the decomposition of the full function for

a response η^{sim} into a sum of functions that only depend on the input variables such that:

$$\eta^{\mathrm{sim}}(\boldsymbol{\theta}) = f(\boldsymbol{\theta}) =$$

$$f_0 + \sum_{i=1}^{N_{\mathrm{param}}} f_i(\theta_i) + \sum_{i=1}^{N_{\mathrm{param}}} \sum_{j=i+1}^{N_{\mathrm{param}}} f_{ij}(\theta_i, \theta_j) + \ldots + f_{12..N_{\mathrm{param}}}(\theta_1, \theta_2, \ldots, \theta_{N_{\mathrm{param}}}) \tag{6}$$

where N_{param} is the number of parameters, i and j index the input parameters and f_0 is the mean value of $f(\boldsymbol{\theta})$. In practical applications, it is possible to truncate the above expression to second-order terms [33]. The order of a group of terms is given the symbol d, with the maximum order considered d_{max}. Thus, a response is approximated by:

$$\eta^{\mathrm{sim}}(\boldsymbol{\theta}) \approx f(\boldsymbol{\theta}) = f_0 + \underbrace{\sum_{i=1}^{N_{\mathrm{param}}} f_i(\theta_i)}_{\text{first-order terms}} + \underbrace{\sum_{i=1}^{N_{\mathrm{param}}} \sum_{j=i+1}^{N_{\mathrm{param}}} f_{ij}(\theta_i, \theta_j)}_{\text{second-order terms}} \tag{7}$$

3.1.1 Calculation of sensitivities

The global sensitivities can be determined by considering the variance of the model response. The first-order variance, $\sigma^2_{\eta^{\mathrm{sim}},i}$, and second-order variance, $\sigma^2_{\eta^{\mathrm{sim}},ij}$, both contribute to this quantity, given by:

$$\sigma^2_{\eta^{\mathrm{sim}},i} = \int_{-1}^{1} f_i(\theta_i)^2 \mathrm{d}\theta_i \tag{8}$$

$$\sigma^2_{\eta^{\mathrm{sim}},ij} = \int_{-1}^{1} \int_{-1}^{1} f_{ij}(\theta_i, \theta_j)^2 \mathrm{d}\theta_i \mathrm{d}\theta_j \tag{9}$$

where the integrals are taken over the upper- and lower-bounds chosen for the parameters, here assumed to be normalised to be $[-1, 1]$. This is consistent with other experimental design literature [2, 20]. The total variance is then given by:

$$\sigma^2_{\eta^{\mathrm{sim}}} = \sum_{i=1}^{N_{\mathrm{param}}} \sigma^2_{\eta^{\mathrm{sim}},i} + \sum_{i=1}^{N_{\mathrm{param}}} \sum_{j=i+1}^{N_{\mathrm{param}}} \sigma^2_{\eta^{\mathrm{sim}},ij} \tag{10}$$

Then, the first- and second-order normalised sensitivities are given by:

$$S_{\eta^{\mathrm{sim}}}(\theta_i) = \frac{\sigma^2_{\eta^{\mathrm{sim}},i}}{\sigma^2_{\eta^{\mathrm{sim}}}} \quad \text{and} \quad S_{\eta^{\mathrm{sim}}}(\theta_i, \theta_j) = \frac{\sigma^2_{\eta^{\mathrm{sim}},ij}}{\sigma^2_{\eta^{\mathrm{sim}}}} \tag{11}$$

That is, $S_{\eta^{\mathrm{sim}}}(\theta_i)$ represents the first-order sensitivity of model response η^{sim} to parameter θ_i, and so on. These quantities can be used to compare the influence of parameters within a particular model response. To compare across model responses, the sensitivity should be converted to an absolute sensitivity. Here, the absolute sensitivity is measured by the standard deviation of the first-order model response:

$$S^*_{\eta^{\mathrm{sim}}}(\theta_i) = \sigma_{\eta^{\mathrm{sim}},i} \tag{12}$$

where $S^*_{\eta^{\mathrm{sim}}}(\theta_i)$ has dimensions $\left[\eta^{\mathrm{sim}}\right]$. Physically, this quantity represents the standard deviation in output response η^{sim} achievable from varying parameter θ_i within its specified bounds.

Start

Calculate f_0
Calculate $\overline{R}^2(f_0)$
$d \leftarrow 0$

$d < d_{\max}$

TRUE

$d \leftarrow d + 1$
$M_d \leftarrow 0$

FALSE

$\overline{R}^2 < \overline{R}^{2*}$

TRUE

FALSE

$M_d < M_{\max,d}$

TRUE

FALSE

$M_d \leftarrow M_d - 1$

$n \leftarrow n + 1$

$M_d \leftarrow M_d + 1, n \leftarrow 0$

TRUE

FALSE

$n = 0$

TRUE

$\delta\overline{R}^2 > \delta\overline{R}^2_{\min}$

for $i_1 \leftarrow 1$ **to** N_{param}:
for $i_2 \leftarrow 1$ **to** $i_1 - 1$:
. . . (nest loops until i_d)
Calculate $\alpha^{n+1}_{i_1 i_2 \ldots i_d, M_d}$

TRUE

for $i_1 \leftarrow 1$ **to** N_{param}:
for $i_2 \leftarrow 1$ **to** $i_1 - 1$:
. . . (nest loops until i_d)
$\alpha^{n+1}_{i_1 \ldots i_d, M_d} \leftarrow \alpha^{n}_{i_1 \ldots i_d, M_d}$

FALSE

$\delta\overline{R}^2 < 0$

$\overline{R}^2_{\text{old}} \leftarrow \overline{R}^2$
Calculate new $\overline{R}^2$
$\delta\overline{R}^2 \leftarrow \overline{R}^2 - \overline{R}^2_{\text{old}}$

Calculate next iteration of response surface

FALSE

Finish

Use previous iteration

Figure 2: *Algorithm for recursive fitting of the polynomials and selection of $\bar{R}^2$.*

3.1.2 Automatic order selection

The functions $f(\theta)$ must be determined in order to evaluate the sensitivities. These functions are decomposed into orthogonal basis functions [19], which are taken as Legendre polynomials. The coefficients of these polynomials are determined through a recursive fitting procedure. This has the advantage of being able to tailor the polynomial order to each of the interaction order functions. Similar approaches have been adopted in the work of Ziehn and Tomlin [43].

The algorithm to conduct this whole fitting process is given in Figure 2. The user specifies a maximum interaction order ($d_{\max}$) and maximum polynomial order for each interaction order ($M_{max,d}$) and the algorithm yields the first polynomial with $\overline{R}^2$ above a tolerance $\overline{R}^{2*}$. A tolerance on the minimum improvement in $\overline{R}^2$, $\overline{R}^2_{\min}$ is applied to increase the efficiency of the process. If a new iteration is found to be worse than the previous one, the new iteration is discarded and the algorithm moves onto the next interaction order.

Table 3: *Experimental datasets used in the present work. d_{type} refers to the physical quantity being measured from the system: either primary (d_{pri}) or mobility (d_{mob}) diameter. The statistical quantity measured for the particle size is given in the column μ_{type}. An asterisk (*) denotes an estimated quantity.*

i	T	y_{SiH_4}	P	τ	d_{type}	μ_{type}	$\eta_i^{exp,\mu}$	$\eta_i^{exp,\sigma}$	Ref.
-	°C	%	kPa	ms	-	-			
1	1100	0.04	2.5	80	d_{pri}	mode	26.7	1.07	[15]
2	1100	0.04	2.5	192	d_{pri}	mean	26.0	1.11	[15]
3	1100	0.125	2.5	192	d_{pri}	mean	38.0	1.28	[15]
4	1100	0.128	2.5	80	d_{pri}	mode	31.0	1.3	[15]
5	1100	0.02	2.5	80	d_{pri}	mode	41.0	1.06	[15]
6	1100	0.08	2.5	80	d_{pri}	mode	24.0	1.25	[15]
7	1100	0.04	2.5	420	d_{pri}	mode	32.5	1.10	[15]
8	900	0.04	2.5	420	d_{pri}	mode	21.2	1.11	[15]
9	1000	0.04	2.5	420	d_{pri}	mode	28.5	1.11	[15]
10	816	0.033	51	2600	d_{pri}	mode	11.0	1.50*	[9]
11	1047	0.033	51	2100	d_{pri}	mode	11.0	1.55*	[9]
12	1307	0.033	51	1800	d_{pri}	mode	15.0	1.54*	[9]
13	1200	0.01	101	1000	d_{mob}	mode	127	1.38*	[42]
14	1050	0.214	20	6	d_{pri}	mean	43.4	-	[8] '630S'
15	1150	0.09	20	15	d_{pri}	mean	55.4	-	[8] '631S'
16	1000	0.06	20	53	d_{pri}	mean	23.0	-	[8] '654S'
17	800	0.001	101	900	d_{mob}	mode	89.0	1.61*	[29]
18	800	0.0004	101	900	d_{mob}	mode	51.0	1.55*	[29]
19	600	0.05	39	870	d_{pri}	mean	52.0	-	[30]

3.2 Analysis procedure

There is a wealth of experimental conditions at which the silicon nanoparticle synthesis model can be evaluated [8, 9, 15, 29, 42]. These are given in Table 3. There, experiments are described by their process conditions: representative temperature (T), initial mole fraction of silane (y_{SiH_4}), total pressure (P) and residence time (τ). The resultant PSDs from such experiments, where available, are described by a modal or average particle size ($\eta_i^{exp,\mu}$), and a geometric standard deviation ($\eta_i^{exp,\sigma}$).

A low-discrepancy (Sobol) sequence was used to evaluate the model at points within the bounds defined for the parameters. This sequence was constructed around the parameter optimals identified in previous work [22]. The modal or mean particle size ($\eta_i^{sim,\mu}$) and the geometric standard deviation ($\eta_i^{sim,\sigma}$) of the ensemble were calculated at each of these points. HDMR response surfaces were determined from this data for the two PSD descriptors.

4 Results and discussion

The HDMR approach to parameter analysis yields the sensitivity of each experimental case to each parameter (first-order) or parameter pair combination (second-order). Only the first-order sensitivities will be discussed here, as it was observed that the only significant second-order interactions were composed of those which were significant in the first-order.

4.1 Breakdown of sensitivities

In Figure 3, the sensitivity of the mode or mean of a PSD is displayed. As there were 19 experimental cases, each with 7 first-order sensitivities, a representative experiment was chosen from each experiment group to simplify visualisation of data. The absolute sensitivities of the PSD mode or mean are first compared across the parameters for each of the 6 groups in Figure 3(a).

It is clearly evident that the particle size is most sensitive to $A_{\mathrm{SR,SiH_4}}$, that is, the surface reaction process. It has the largest absolute sensitivity for each of the representative experimental cases. This confirms the importance of accurately describing surface reaction process in models for silicon nanoparticle formation. The second most sensitive parameter is $A_{1,\mathrm{LP}}$, the silane decomposition pre-exponential. This is not surprising, as it has often been targeted for optimisation in previous studies [16, 24].

In Figure 3(b), the first-order sensitivities are compared within experiments. Again, it is evident that the surface reaction pre-exponential is the dominant parameter for all cases. However, the relative importance $A_{1,\mathrm{LP}}$ and to a lesser extent, $A_{3,\mathrm{LP}}$ and $A_{\mathrm{H_2}}$ are seen here. It is interesting to observe that $A_{\mathrm{H_2}}$ accounts for approximately 5% of the sensitivity for the cases of Frenklach et al. [9] and Onischuk et al. [30], as both cases were experimentally reported to yield particles with high concentrations of hydrogen.

The sensitivities are broken-down differently when considering sensitivity of the PSD's geometric standard deviation, shown in Figure 4. Again, the model is most sensitive to $A_{\mathrm{SR,SiH_4}}$, $A_{1,\mathrm{LP}}$ and less so $A_{3,\mathrm{LP}}$, $A_{\mathrm{H_2}}$, depicted in Figure 4(a). However, the internal breakdown of sensitivities is quite different. It is illustrated in Figure 3(b) that $A_{1,\mathrm{LP}}$ plays an important role for all experimental cases. Since $A_{1,\mathrm{LP}}$ has a large impact on the inception process of particles, this observation reinforces the conclusions of Nguyen and Flagan [29] and Körmer et al. [16] that controlling the nucleation rate is critical in controlling the dispersion of particles.

Further, the absolute sensitivities with respect to geometric standard deviation are generally greatest for the cases of Flint et al. [8], Nguyen and Flagan [29] and Onischuk et al. [30] (Figure 4(a)). These three cases correspond to those where aggregate particles are formed, where the coagulation rate is likely to be high. In such systems, it is common to see a spike in geometric standard deviation prior to it reaching its final value - either controlled by a finite sintering rate or primary coalescence [23]. It is therefore suggested that by varying the parameters describing inception, the PSD's geometric standard deviation has been observed at different points along this process, leading to an increased sensitivity of the distribution width for aggregate-forming cases.
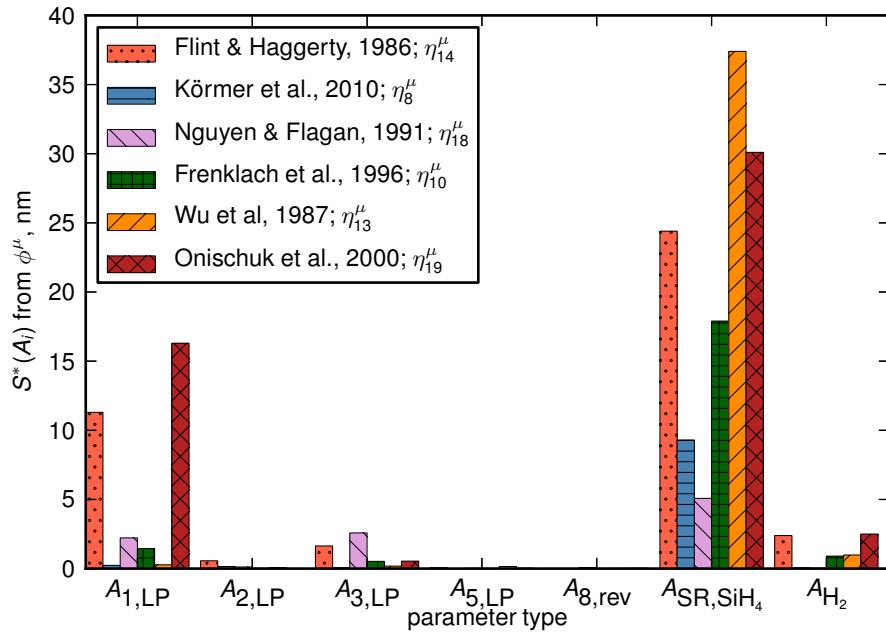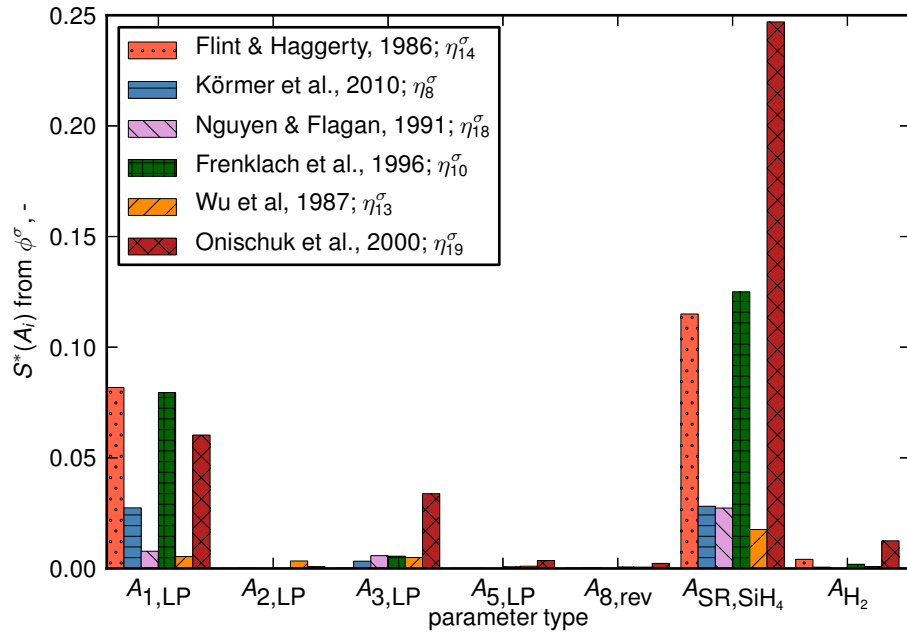
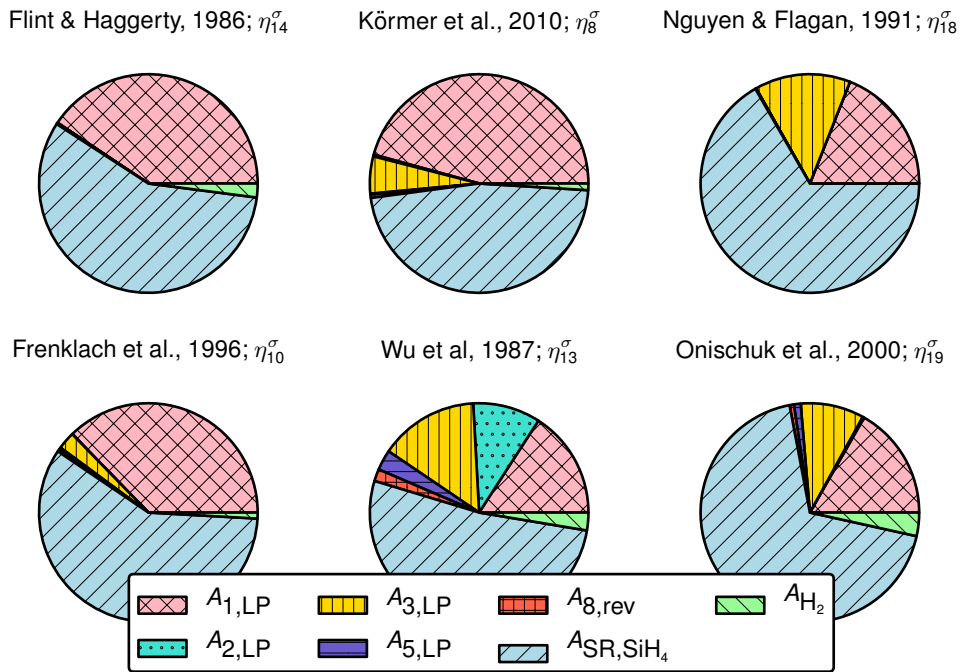(a) The absolute sensitivities of the PSD mode compared across parameter types
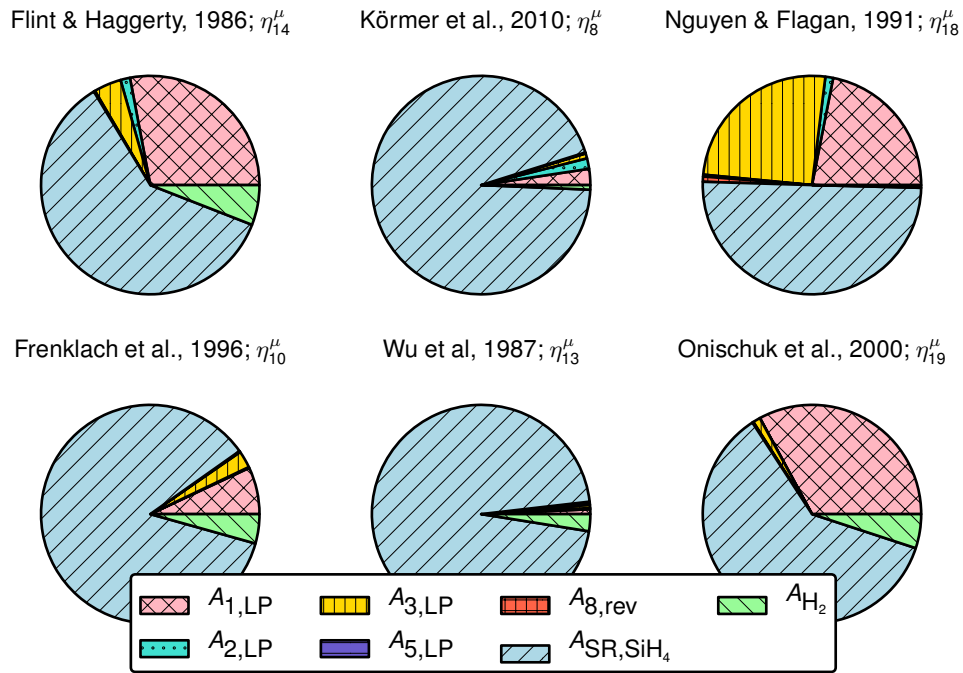
(b) The normalised sensitivities of the PSD mode compared across experiments

Figure 3: *Comparison of the sensitivity of the PSD mode/mean (μ case) across parameter types and different representative experiments.*

12

(a) The absolute sensitivities of the PSD geometric standard deviation compared across parameter types

(b) The normalised sensitivities of the PSD geometric standard deviation compared across experiments

Figure 4: *Comparison of the sensitivity of the PSD geometric standard deviation (σ case) across parameter types and different representative experiments.*

Finally, the case with the least sensitive geometric standard deviation is that of Wu et al. [42]. In this case, spherical particles are produced in a very hot reactor. It is likely that due to fast sintering [23] and strong particle nucleation [22], the system reaches the self-preserving PSD for the majority of parameter combinations. Thus, while the modal point of the PSD is very sensitive to surface growth (Figure 3(a)), the comparative width of the distribution is relatively static (Figure 3(a)).

4.2 Sensitivities as a function of process conditions

In the previous section, the sensitivity the model at specific experimental conditions was addressed. The HDMR results can also be used to investigate how sensitivity varies with the process conditions across all experiments. In order to do this, the absolute sensitivities were plotted on a bubble plot in Figure 5, where the size of the circle is proportional to the sensitivity.

The left column of Figure 5 shows the sensitivity of the particle size descriptor, while the sensitivity of the geometric standard deviation is given in the right column. The choice of temperature and initial silane pressure (Py_{SiH_4}) was made to clearly separate the experimental cases, although in practice the experiments are actually functions of more variables–such as residence time and reactor configuration–than these two. In any case, the clear importance of the surface reaction process at all process conditions is again demonstrated here.

It appears that $A_{3,\text{LP}}$ is generally more important at lower pressures. This could indicate the the reaction pathway for forming Si_2H_6 becomes more important as silane pressure decreases. This observation would be consistent with homogeneous nucleation theory, as the critical cluster size increases as the partial pressure of silicon decreases. That is, larger gas-phase clusters (e.g. Si_2H_6+) must be formed before particles are stable enough to grow. Hence, the parameter describing one of the major pathways for this process has a stronger effect on PSD characteristic at lower silane pressure.

There are also some trends within experimental cases. For example, it is evident in the cases of Körmer et al. [16] that the sensitivity with respect to geometric standard deviation is roughly inversely proportional to silane pressure, while direct proportionality is observed for PSD mode sensitivity. This phenomenon is consistent with the experiments of Körmer et al. [15], where increasing the pressure of silane would cause runaway nucleation, yielding broader PSDs and larger particles. Thus, as the pressure increases and the PSD broadens, the system nears the self-preserving distribution and the PSD's geometric standard deviation becomes insensitive to input parameters.

5 Conclusions

This paper has presented an adaptation of a High Dimensional Model Representation (HDMR) to a detailed model for silicon nanoparticle synthesis. The HDMR yielded information about the sensitivity of the model outputs to various input parameters across a range of experiments conditions and configurations. The output responses investigated
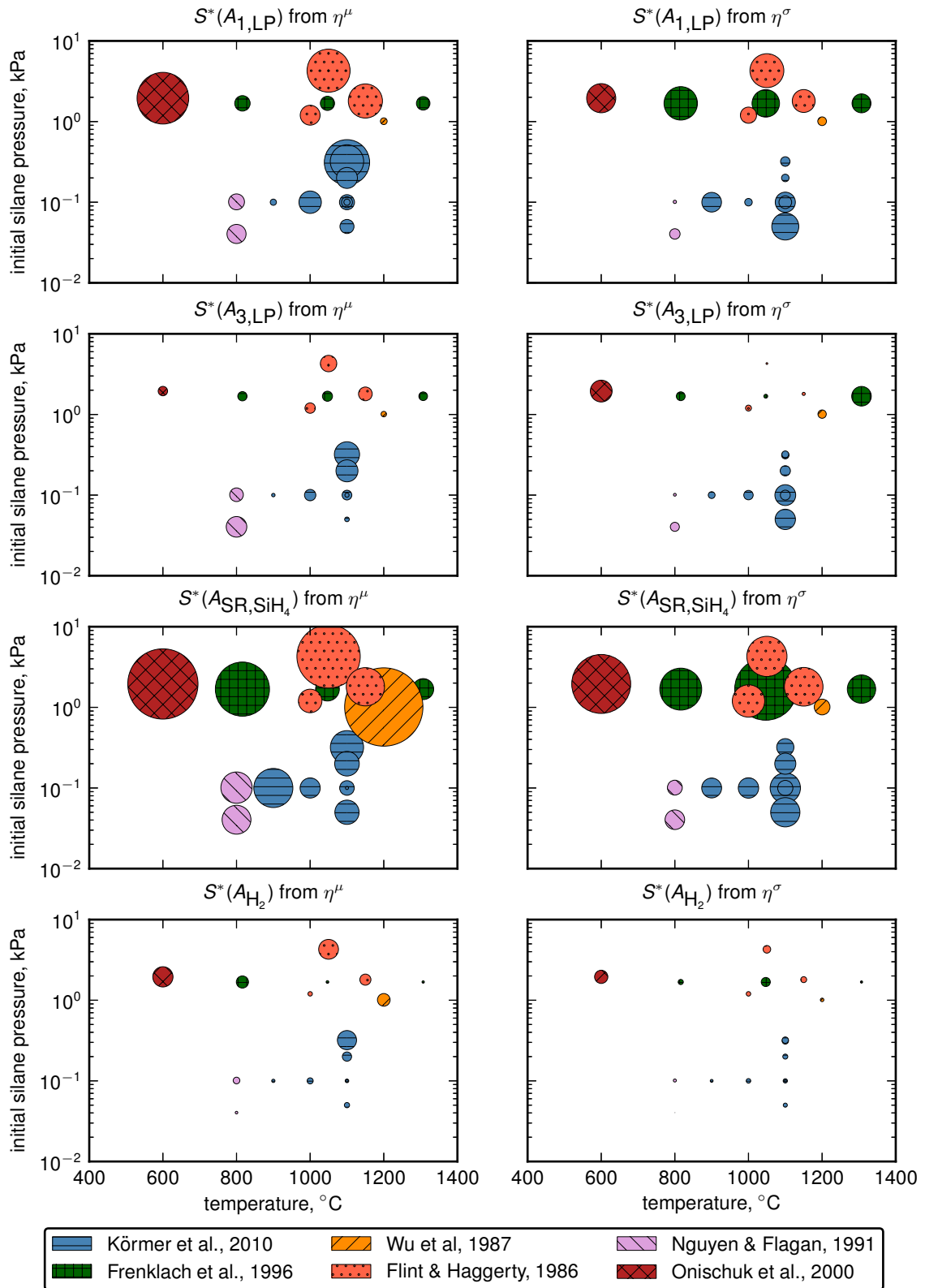
Figure 5: *Global sensitivities (S^*) for $A_{1,LP}$, $A_{3,LP}$, A_{SR,SiH_4}, A_{H_2} shown as a function of process conditions. Each circle represents an experimental case (Table 3) and its diameter is proportional to the absolute sensitivity.*

were the particle size and distribution width, the latter represented as geometric standard deviation.

It was found that the particle size was most sensitive to the parameter controlling the surface reaction rate. The same was observed for the geometric standard deviation, however it was also sensitive to the initial decay rate of silane. The sensitivity analysis data could also be linked to phenomena reported experimentally. For example, the model was shown to be sensitive to the hydrogen release rate in cases where high concentrations of hydrogen were experimentally reported.

The knowledge of the model's sensitivity can now be applied to embark on an experimental discrimination pathway. This can potentially indicate which experiments pull parameter optimals in which directions. Alternatively, it can show which experiments–or the model's representation of them–are incorrect. Although these aspects remain to be completed, it has been demonstrated that use of a HDMR as part of parameter estimation procedure can reveal new layers of insight from a complex model.

6   Acknowledgements

References

[1] M. Balthasar and M. Kraft. A stochastic approach to calculate the particle size distribution function of soot particles in laminar premixed flames. *Combustion and Flame*, 133(3):289–298, 2003.

[2] A. Braumann, M. Kraft, and P. Mort. Parameter estimation in a multidimensional granulation model. *Powder Technology*, 197(3):196–210, 2010.

[3] A. Braumann, P. L. W. Man, and M. Kraft. The inverse problem in granulation modeling–Two different statistical approaches. *AIChE Journal*, 57(11):3105–3121, 2011.

[4] W. R. Cannon, S. C. Danforth, J. H. Flint, J. S. Haggerty, and R. A. Marra. Sinterable ceramic powders from laser-driven reactions: I, Process description and modeling. *Journal of the American Ceramic Society*, 65(7):324–330, 1982.

[5] M. Celnik, R. Patterson, M. Kraft, and W. Wagner. Coupling a stochastic soot population balance to gas-phase chemistry using operator splitting. *Combustion and Flame*, 148(3):158–176, 2007.

[6] D. Chen, Z. Zainuddin, E. Yapp, J. Akroyd, S. Mosbach, and M. Kraft. A fully coupled simulation of PAH and soot growth with a population balance model. *Proceedings of the Combustion Institute*, 34:1827–1835, 2013.

[7] A. Eibeck and W. Wagner. An efficient stochastic algorithm for studying coagulation dynamics and gelation phenomena. *SIAM Journal on Scientific Computing*, 22(3): 802–821, 2001.

[8] J. H. Flint, R. A. Marra, and J. S. Haggerty. Powder temperature, size, and number density in laser-driven reactions. *Aerosol Science and Technology*, 5(2):249–260, 1986.

[9] M. Frenklach, L. Ting, H. Wang, and M. J. Rabinowitz. Silicon particle formation in pyrolysis of silane and disilane. *Israel Journal of Chemistry*, 36(3):293–303, 1996.

[10] M. Goodson and M. Kraft. An efficient stochastic algorithm for simulating nano-particle dynamics. *Journal of Computational Physics*, 183(1):210–232, 2002.

[11] P. Ho, M. E. Coltrin, and W. G. Breiland. Laser-induced fluorescence measurements and kinetic analysis of Si atom formation in a rotating disk chemical vapor deposition reactor. *The Journal of Physical Chemistry*, 98(40):10138–10147, 1994.

[12] W. G. Houf, J. F. Grcar, and W. G. Breiland. A model for low pressure chemical vapor deposition in a hot-wall tubular reactor. *Materials Science and Engineering: B*, 17(1-3):163–171, 1993.

[13] C. A. Kastner, A. Braumann, P. L. W. Man, S. Mosbach, G. P. E. Brownbridge, J. Akroyd, M. Kraft, and C. Himawan. Bayesian parameter estimation for a jet-milling model using metropolis-hastings and wang-landau sampling. *Chemical Engineering Science*, 89:244–257, 2013.

[14] J. Knipping, H. Wiggers, B. Rellinghaus, P. Roth, D. Konjhodzic, and C. Meier. Synthesis of high purity silicon nanoparticles in a low pressure microwave reactor. *Journal of Nanoscience and Nanotechnology*, 4(8):1039–1044, 2004.

[15] R. Körmer, M. P. M. Jank, H. Ryssel, H. J. Schmid, and W. Peukert. Aerosol synthesis of silicon nanoparticles with narrow size distribution–Part 1: Experimental investigations. *Journal of Aerosol Science*, 41(11):998–1007, 2010.

[16] R. Körmer, H. J. Schmid, and W. Peukert. Aerosol synthesis of silicon nanoparticles with narrow size distribution–Part 2: Theoretical analysis of the formation mechanism. *Journal of Aerosol Science*, 41(11):1008–1019, 2010.

[17] M. Kraft and S. Mosbach. The future of computational modelling in reaction engineering. *Philosophical Transactions of the Royal Society A*, 368(1924):3633–3644, 2010.

[18] P. Lavvas, M. Sander, M. Kraft, and H. Imanaka. Surface chemistry and particle shape: Processes for the evolution of aerosols in titan's atmosphere. *The Astrophysical Journal*, 728(2):80, 2011.

[19] G. Li, S.-W. Wang, and H. Rabitz. Practical approaches to construct RS-HDMR component functions. *The Journal of Physical Chemistry A*, 106(37):8721–8733, 2002.

[20] P. Man, A. Braumann, and M. Kraft. Resolving conflicting parameter estimates in multivariate population balance models. *Chemical Engineering Science*, 65(13): 4038–4045, 2010.

[21] L. Mangolini. Synthesis, properties, and applications of silicon nanocrystals. *Journal of Vacuum Science & Technology B*, 31(2):020801, 2013.

[22] W. J. Menz and M. Kraft. A new model for silicon nanoparticle synthesis. *Combustion and Flame*, 160:947–958, 2013.

[23] W. J. Menz and M. Kraft. The suitability of particle models in capturing aggregate structure and polydispersity. *Aerosol Science & Technology*, 47:734–745, 2013.

[24] W. J. Menz, S. Shekar, G. Brownbridge, S. Mosbach, R. Körmer, W. Peukert, and M. Kraft. Synthesis of silicon nanoparticles with a narrow size distribution: A theoretical study. *Journal of Aerosol Science*, 44:46–61, 2012.

[25] W. J. Menz, R. I. A. Patterson, W. Wagner, and M. Kraft. Application of stochastic weighted algorithms to a multidimensional silica particle model. *Journal of Computational Physics*, 248:221–234, 2013.

[26] N. M. Morgan, C. G. Wells, M. J. Goodson, M. Kraft, and W. Wagner. A new numerical approach for the simulation of the growth of inorganic nanoparticles. *Journal of Computational Physics*, 211(2):638–658, 2006.

[27] S. Mosbach, A. Braumann, P. L. W. Man, C. A. Kastner, G. P. E. Brownbridge, and M. Kraft. Iterative improvement of bayesian parameter estimates for an engine model by means of experimental design. *Combustion and Flame*, 159(3):1303–1313, 2012.

[28] T. Murthy, N. Miyamoto, M. Shimbo, and J. Nishizawa. Gas-phase nucleation during the thermal decomposition of silane in hydrogen. *Journal of Crystal Growth*, 33(1):1–7, 1976.

[29] H. V. Nguyen and R. C. Flagan. Particle formation and growth in single-stage aerosol reactors. *Langmuir*, 7(8):1807–1814, 1991.

[30] A. A. Onischuk, A. I. Levykin, V. P. Strunin, K. K. Sabelfeld, and V. N. Panfilov. Aggregate formation under homogeneous silane thermal decomposition. *Journal of Aerosol Science*, 31(11):1263–1281, 2000.

[31] R. I. A. Patterson, J. Singh, M. Balthasar, M. Kraft, and J. R. Norris. The linear process deferment algorithm: A new technique for solving population balance equations. *SIAM Journal on Scientific Computing*, 28(1):303, 2006.

[32] E. L. Petersen and M. W. Crofton. Measurements of high-temperature silane pyrolysis using SiH_4 IR emission and SiH_2 laser absorption. *The Journal of Physical Chemistry A*, 107(50):10988–10995, 2003.

[33] H. Rabitz and Ö. F. Ali̇ş. General foundations of high-dimensional model representations. *Journal of Mathematical Chemistry*, 25(2-3):197–233, 1999.

[34] M. Sander, R. H. West, M. S. Celnik, and M. Kraft. A detailed model for the sintering of polydispersed nanoparticle agglomerates. *Aerosol Science and Technology*, 43(10):978–989, 2009.

[35] S. Shekar, W. J. Menz, A. J. Smith, M. Kraft, and W. Wagner. On a multivariate population balance model to describe the structure and composition of silica nanoparticles. *Computers & Chemical Engineering*, 43:130–147, 2012.

[36] S. Shekar, A. J. Smith, W. J. Menz, M. Sander, and M. Kraft. A multidimensional population balance model to describe the aerosol synthesis of silica nanoparticles. *Journal of Aerosol Science*, 44:83–98, 2012.

[37] K. Sinniah, M. G. Sherman, L. B. Lewis, W. H. Weinberg, J. T. Yates Jr, and K. C. Janda. Hydrogen desorption from the monohydride phase on Si (100). *The Journal of Chemical Physics*, 92:5700, 1990.

[38] M. T. Swihart and S. L. Girshick. Thermochemistry and kinetics of silicon hydride cluster formation during thermal decomposition of silane. *The Journal of Physical Chemistry B*, 103(1):64–76, 1999.

[39] A. Tomlin. The role of sensitivity and uncertainty analysis in combustion modelling. *Proceedings of the Combustion Institute*, 34(1):159–176, 2013.

[40] A. Vikhansky and M. Kraft. A Monte Carlo methods for identification and sensitivity analysis of coagulation processes. *Journal of Computational Physics*, 200(1):50–59, 2004.

[41] A. Vikhansky and M. Kraft. Two methods for sensitivity analysis of coagulation processes in population balances by a Monte Carlo method. *Chemical Engineering Science*, 61(15):4966–4972, 2006.

[42] J. J. Wu, H. V. Nguyen, and R. C. Flagan. A method for the synthesis of submicron particles. *Langmuir*, 3(2):266–271, 1987.

[43] T. Ziehn and A. Tomlin. Global sensitivity analysis of a 3D street canyon model–Part I: The development of high dimensional model representations. *Atmospheric Environment*, 42(8):1857–1873, 2008.